Department of Applied Mathematics
Faculty of EEMCS

University of Twente
The Netherlands

P.O. Box 217
7500 AE Enschede
The Netherlands
Phone: +31-53-4893400
Fax: +31-53-4893114
Email: memo@math.utwente.nl
www.math.utwente.nl/publications

Memorandum No. 1775

Extension of a discontinuous Galerkin finite element method to viscous rotor flow simulations

H. van der Ven[1], O.J. Boelens[1],
C.M. Klaij and J.J.W. van der Vegt

August, 2005

ISSN 0169-2690

[1]Netherlands National Aerospace Laboratory NLR, P.O. Box 90502, 1006 BM Amsterdam, The Netherlands

Extension of a discontinuous Galerkin finite element method to viscous rotor flow simulations

H. van der Ven and O.J. Boelens *
Netherlands National Aerospace Laboratory NLR
P.O. Box 90502, 1006 BM Amsterdam, The Netherlands
{venvd, boelens}@nlr.nl

C.M. Klaij and J.J.W. van der Vegt †
University of Twente, Department of Applied Mathematics
P.O. Box 217, 7500 AE Enschede, The Netherlands
{c.m.klaij, j.j.w.vandervegt}@math.utwente.nl

Abstract

Heavy vibratory loading of rotorcraft is relevant for many operational aspects of helicopters, such as the structural life span of (rotating) components, operational availability, the pilot's comfort, and the effectiveness of weapon targeting systems. A precise understanding of the source of these vibrational loads has important consequences in these application areas. Moreover, in order to exploit the full potential offered by new vibration reduction technologies, current analysis tools need to be improved with respect to the level of physical modeling of flow phenomena which contribute to the vibratory loads. In this paper, a computational fluid dynamics tool for rotorcraft simulations based on first-principles flow physics is extended to enable the simulation of viscous flows. Viscous effects play a significant role in the aerodynamics of helicopter rotors in high-speed flight. The new model is applied to three-dimensional vortex flow and laminar dynamic stall. The applications clearly demonstrate the capability of the new model to perform on deforming and adaptive meshes. This capability is essential for rotor simulations to accomodate the blade motions and to enhance vortex resolution.
Keywords: compressible Navier-Stokes equations, discontinuous Galerkin finite element methods, viscous rotor flow
Mathematics Subject Classification: 35L65, 65M60, 76D05, 76D17, 76M10

*Research funded by NLR's basic research programme.
†Research conducted in the STW project TWI.5541; the financial support from STW and NLR is gratefully acknowledged.

Symbols and abbreviations

a_∞	freestream speed of sound
α	angle of attack
BVI	Blade-Vortex Interaction
c	chord
CFD	Computational Fluid Dynamics
DG	discontinuous Galerkin
MTMG	Multitime-Multigrid
ω	vorticity
RANS	Reynolds-averaged Navier-Stokes
u	velocity vector
u_j	j-th component of a vector
$u_{,j}$	$\frac{\partial u}{\partial x_j}$
$\hat{U}_j^i$	expansion coefficient for the j-th basis function and the i-th conservative variable
∇	$\nabla_j = \frac{\partial}{\partial x_j}$
$.^T$	transpose of a vector

1 Introduction

The high vibrational loading of rotorcraft is an important contributor to maintenance issues of rotorcraft and affects its operational availability. A precise understanding of the sources of these vibrational loads has important consequences for helicopter design, safety and costs, cabin comfort, and weapon targeting effectiveness (see for instance the references in [15]). Concerning helicopter design, O. Dieterich, from Eurocopter, mentions the following in his ERF 2005 overview article [4] on vibrational analysis for rotorcraft: "(...) the full vibration reduction potential offered by advantageous rotor and airframe design can not be exploited at the moment by industry due to the shortcomings of current vibration prediction technology." The reasons offered for these shortcomings are uncertainties in the accuracy of the prediction tools caused by the relatively small vibratory loads compared to the overall thrust and the multi-disciplinary nature of the aero-elastic problem, complicating identification of those model components which need improvement.

The call for increased accuracy in the prediction of vibratory loads can in principle be answered by models based on first-principles physics. Promising results have been obtained by several authors, for example Pahlke et al. [10], Pomin et al. [11], and Servera et al. [13], all applying an aerodynamical model based on first-principles physics using computation fluid dynamics (CFD) methods.

There are two flight regimes where the vibratory levels exceed the acceptable level of 0.05g. The first is during low-speed flight (descent, maneuver) where the blades encounter the wake of the preceding blades (BVI). The second is during high-speed flight (cruise, typically above one hundred knots) where the aerodynamics of a single blade leads to strong pressure fluctuations. These fluctuations are both caused by compressibility effects (shocks) on the advancing side, and strong viscous effects (dynamic stall) on the retreating side.

From an aerodynamic point of view, blade-vortex interaction and shocks can be sufficiently resolved using an inviscid flow model. The physics of dynamic stall on the retreating side, however, is not contained in the Euler equations. This is one of the reasons to consider viscous flows in this paper. The complexity of the dynamic stall phenomenom, however, should not be underestimated. The study of dynamic stall is an active field of research, even for fixed-wing applications (see for instance Hansen et al. [5]). So a step-wise approach is followed, and first applications will concern the laminar vortex generated by the sharp leading edge of a delta wing and the laminar dynamic stall of a NACA0012 foil in rapid pitch-up maneuver. These examples serve as a demonstration of the capabilities of the numerical method.

Since accurate rotor flow simulation requires correct blade motions, aero-elastic simulations need to be performed. So one should also consider the importance of the viscous effects for fluid-structure interaction. Pahlke et al. [9] and Pomin at al. [11] perform aero-elastic simulations for rotors in high-speed forward flight and they both concluded that in order to correctly predict the sectional moments, it is necessary to take into account the viscous effects. Pahlke et al. [9] apply a so-called weak fluid-structure coupling where the blade motions are obtained from an aeromechanical code correcting the aerodynamic forces of the aeromechanical code with the forces computed in the CFD simulation. Pomin et al. [11] apply a strong coupling, which increased the computational complexity of the problem in such a way that the rotor system could not be trimmed. Although the authors do not provide a reason for the importance of the viscous contribution to the sectional moments, it is suspected to be caused by the fact that for high-speed forward flight the collective pitch is of the order of fifteen degrees. At such angles, viscous effects determine the flow separation location, which cannot be predicted using an inviscid flow model. Since the sectional moments influence the blade motion, it seems that for aero-elastic simulations of rotor systems viscous simulations are necessary to correctly predict the blade motion, at least for high-speed flight. This is another reason to study viscous flow simulation for rotorcraft.

Apart from the flow model, the simulation of rotorcraft flow requires that the CFD method allows deforming meshes to accomodate for the rigid and elastic blade motions. Moreover, since for many flight conditions the rotor encounters its own wake, accurate vortex capturing is necessary to resolve the wake-blade interactions such as BVI. The vortex capturing capabilities of CFD methods can be increased by either increasing the order of accuracy of the discretization or increasing the mesh resolution near the vortices. For the latter, a local grid refinement capability of the CFD method is required.

The numerical method used in this paper is based on the space-time discontinuous Galerkin (DG) finite element method. Recently, DG methods have received a lot of attention (see Cockburn et al. [3] for an overview) due to the following favourable characteristics of the method:

- the method is extremely local (only data from cell neighbours is required) and consequently allows local grid refinement to resolve local phenomena such as tip vortices,
- being a finite element method there is a solid mathematical base for a posteriori error analysis,
- higher order accuracy is conceptually easy to accomplish without jeopardizing the other favourable characteristics of the method,
- the locality of the method makes parallelization easy and scalable,
- the space-time formulation is a conservative scheme for arbitrarily moving bodies (such as rotor blades) on deforming (and adaptive) grids, and the locality of the method allows the generally non-smooth meshes resulting from grid deformation.

The DG method has successfully been applied to inviscid rotor simulations. Boelens et al. [2] have demonstrated the vortex capturing capabilities on locally refined meshes for the simulation of the Operational Loads Survey rotor in forward flight. Van der Ven et al. [15] have extended the method to aero-elastic simulations for rotor systems in forward flight. A revolutionary solution algorithm, MTMG, is used in [15], solving the dynamics of the rotor system in space and time simultaneously. This approach turns a dynamic problem into a steady problem, reducing the computational complexity of simulations of trimmed rotor systems with elastic blades by two orders of magnitude. This solution algorithm is independent of the type of equations being solved, hence its benefits will be unaffected by changing the aerodynamical model from the Euler equations to the Navier-Stokes equations.

The structure of the paper is as follows. First, the numerical method is briefly described. Second, results are presented for a laminar three-dimensional vortex and two-dimensional laminar dynamic stall. Finally, conclusions are drawn.

2 The discontinuous Galerkin finite element method

2.1 General description The discontinuous Galerkin finte element method as developed by Cockburn [3] uses a discontinuous function space to approximate the exact solution of the equations. The method is a mixture of an upwind finite volume and a finite element method. In the current discretization, the flow domain is discretized into a large number of hexahedral elements. The polynomial expansion of the flow field variables are purely element-based and there will be, in general, a discontinuity in the flow field variables across element faces, with as magnitude the truncation error in the polynomial expansion; in the current discretization second order in the mesh width.

To be more precise, the discretized flow state U_h restricted to an element K in the tesselation of the flow domain is given by

$$U_{h|K} = \sum \hat{U}_k \psi_k,$$

where $\{\psi_k | k = 0, 1, \ldots, n\}$ is a set of basis functions. The number n of basis functions depends on the order of accuracy and the space dimension. The first basis function ψ_0 is the constant function. The first expansion coefficient represents the cell-averaged solution $|K|^{-1} \int_K U dx$. The other expansion coefficients are related to the flow gradients according to the formula

$$\frac{\partial U_h}{\partial x_k}_{|K} = 2\hat{U}_k / h_k$$

(on Cartesian meshes), where h_k is the mesh width in the k-direction. Hence, the flow state derivatives are independent variables in the DG discretization, and as a consequence, the vorticity can be directly expressed in independent variables, without the need to construct flow gradients.

2.2 Space-Time discretization for moving bodies Van der Vegt et al. [14] extended the DG discretization to a space-time method. The space-time method discretizes the flow equations on four-dimensional space-time elements. The four-dimensional elements consist of an element at a certain time level and of the same element, possibly moved or deformed, at the next time level. The derivation of the DG discretization proceeds as usual, but now time is treated like space, and one of the flow gradients represents the time derivative of the flow states. The important advantage of space-time methods is that a conservative discretization is obtained on moving and deforming meshes. As explained in the introduction, this is a prerequisite for rotor simulations.

The space-time DG method has been applied to the simulation of the Operational Loads Survey rotor [2]. Local grid refinement has been applied on the deforming mesh to improve the vortex resolution. An impression of the complex vortex system is presented in Figure 1.

2.3 Space-time DG for the Navier-Stokes equations In this section an overview of the DG discretization of the Navier-Stokes equations is presented. Details can be found in Klaij et al. [6].

The Navier-Stokes equations are given by

$$\frac{\partial U}{\partial t} + \nabla \cdot F^e(U) + \nabla \cdot F^v(U, \nabla U),$$

where $U = (\rho, \rho u, \rho E)^T \in \mathbb{R}^5$ is the vector of conservative variables, consisting of density, momentum, and total energy. The viscous flux F^v is given by

$$F^v_k = \begin{pmatrix} 0 \\ \tau_{jk} \\ \tau_{jk} u_j - q_k \end{pmatrix},$$

with $1 \leq j, k \leq 3$. The local stress tensor τ is defined as $\tau_{jk} = \lambda u_{i,i} \delta_{jk} + \mu(u_{j,k} + u_{k,j})$ (μ dynamic viscosity coefficient and λ the diffusivity coefficient). The heat flux vector q_k is given by $q_k = -\kappa T_{,k}$, with κ the thermal

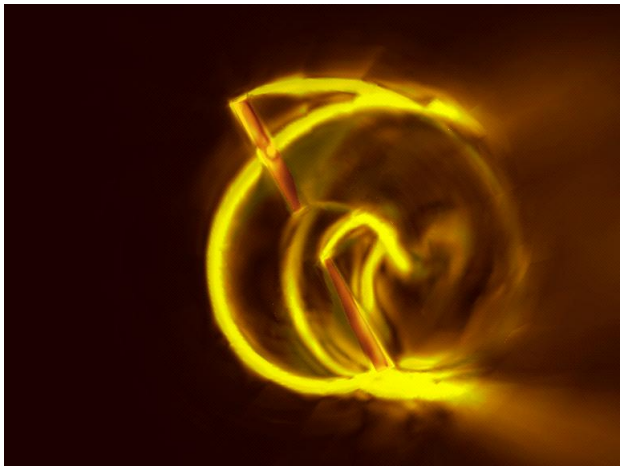

Figure 1: Simulation of the inviscid flow around the Operational Loads Survey rotor in forward flight ($M_{\text{tip}} = 0.664$, $\mu = 0.164$, $C_T = 0.0054$). Vorticity magnitude (between zero and one) at an azimuth of 135^o. Taken from Boelens et al. [2]

conductivity coefficient and T the temperature. The equations are closed using the equation of state for a perfect gas.

In the space-time formulation, the time-derivative and the inviscid flux are written as the divergence of the four-dimensional flux vector $(U, F^e + F^v)^T$. As in standard finite element methods, the equations are rewritten in the weak formulation and after applying Gauss' theorem, face integrals of this flux occur. Because of the discontinuity of the flow representation across element faces, the flux is not uniquely defined. For the flux in the time direction a standard upwind flux is taken (information only flows in the positive time direction). For the spatial inviscid flux, the discontinuity is considered as input for a Riemann problem, and the HLLC approximate Riemann solver is used. More details on the space-time DG discretization of the inviscid flow equations can be found in [14].

Of importance to the derivation of the DG discretization for the Navier-Stokes equations is the following property of the viscous flux:

$$F^v_{ik}(U, \nabla U) = A_{ikrs}(U)U_{r,s}.$$

In other words, the viscous flux is linear in the flow gradients. As explained in Section 2.1 the DG discretization contains the flow gradients as independent variables, so this property will be exploited in the discretization of the Navier-Stokes equations.

Since the flow representation in the DG method is discontinuous across element faces, the concepts of jumps and averages across cell faces is introduced. Given two elements K^L and K^R connecting at a face S, let U^L, resp. U^R, be the restriction of the flow states from the left cell K^L, resp. from the right cell K^R to the face S. Let n be the face normal pointing outwards from the left cell. The jump $[\![U]\!]$ at the face S is defined as

$$[\![U]\!]_k = (U^L - U^R)n_k,$$

and the average $\{\!\{U\}\!\}$ is defined as

$$\{\!\{U\}\!\} = \frac{1}{2}(U^L + U^R).$$

Note that the jump operator is vector-valued.

Let ψ_l be one of the basis functions in the DG discretization, described in Section 2.1, with support in an element K in the tesselation of the computational domain. Ignoring the boundary terms for simplicity of presentation, the DG discretization of the viscous terms in the Navier-Stokes equations contributing to the

equation for the expansion coefficient $\hat{U}_l^i$ is (see [6] for details):

$$
\begin{aligned}
&+ \int_K \psi_{l,k} A_{ikrs} U_{r,s} dx \\
&- \sum_S \int_S [\![\psi_l]\!]_k \{\!\{ A_{ikrs} U_{r,s} \}\!\} dx \\
&- \sum_S \int_S \{\!\{ \psi_{l,k} A_{ikrs} \}\!\} [\![U_r]\!]_s dx \\
&+ \eta \sum_S \int_S [\![\psi_l]\!]_k R_{ik}^S(U) dx,
\end{aligned}
$$

where the sums are taken over all faces connecting to the element K. Because the jumps and averages only require data from neighbouring elements the locality of the discretization is clear.

The first two lines in the above discretization are the basic terms in the discretization. They immediately follow from a weak formulation of the equations and using the DG flow representation to obtain the flow gradients. The discontinuity at the cell faces is simply treated by taking the average of the viscous fluxes from the left and from the right (viscosity has no preferred direction). The last two lines are stabilization terms, penalizing jumps in the solution, without affecting the order of accuracy of the discretization. The so-called lifting operator R^S is not further explained, but is essential for stability. The value of the stabilization parameter η is 7 for three-dimensional flows.

For scalar diffusion, $A_{ikrs} = \nu \delta_{ir} \delta_{ks}$, on a Cartesian mesh the discretization simplifies to

$$
\begin{aligned}
&+ \nu \int_K \psi_{l,k} U_{i,k} dx \\
&- \nu \sum_S \int_S [\![\psi_l]\!]_k \{\!\{ U_{i,k} \}\!\} dx \\
&- \nu \sum_S \int_S \{\!\{ \psi_{l,k} \}\!\} [\![U_i]\!]_k dx \\
&+ \nu\eta \sum_S \int_S [\![\psi_l]\!]_k [\![U_i]\!]_k / h_k dx,
\end{aligned}
$$

where h_k is the mesh width in the k-direction of cell K. In this simplification the symmetry between the second and third line becomes more obvious. For this specific case, we have $R_{ik}^S(U) = [\![U_i]\!]_k / h_k$. Since $\psi_{l,k} = 2\delta_{lk}/h_k$ on a Cartesian mesh, the two stabilization terms are actually the same, and reduce to $+\nu(\eta - 1)\delta_{lk} \sum_S \int_S \{\!\{ \psi_{l,k} \}\!\} [\![U_i]\!]_k dx$.

3 Results

3.1 Vortex over a delta wing Since vortices play an important role in rotor aerodynamics, first laminar steady vortices are studied, generated by the sharp leading edge of a delta wing. The 85^o delta wing of the experiments of Riley and Lowson [12] is considered at a Reynolds number of 40,000, Mach number 0.3 and angle of attack 12.5^o.

Simulations have been performed using both the viscous DG flow solver Hexadap and, for comparison, the finite volume flow solver ENFLOW [7]. A coarse and a fine mesh have been generated, containing 208,000, resp. 1,664,000 cells. The coarse mesh is only used for the simulations with the DG flow solver and has been refined to improve vortex resolution. A cell is refined whenever the vorticity magnitude is greater than $2a_\infty/c$ and the mesh width is greater than $0.01c$. The final adapted mesh contains 347,000 cells. The grid resolution and vortex resolution (in terms of total pressure loss at a cross section at 60% chord) between the DG and finite

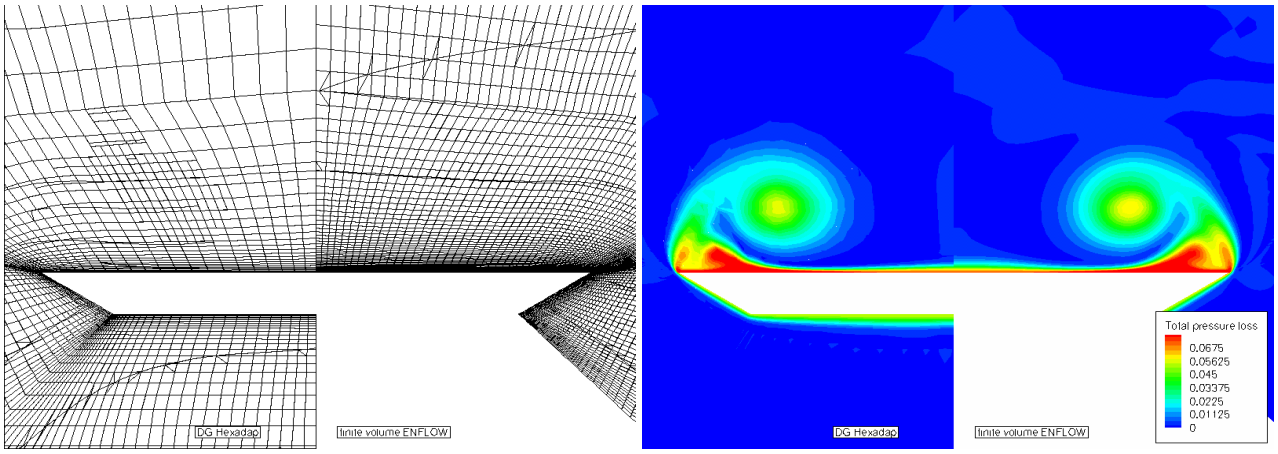

(a) meshes

(b) total pressure loss

Figure 2: Vortex flow over a delta wing (Re=40,000, M=0.3, $\alpha = 12.5^o$). Comparison of vortex resolution at a cross section of 60% chord between the DG solver Hexadap (left) and the finite volume solver ENFLOW (right). The different meshes are shown on top, and the flow results on the bottom. For the ENFLOW results not the complete cross section is shown.

volume simulations is compared in Figure 2. Clearly, the DG solver displays very similar results to the well-verified finite volume flow solver ENFLOW. Figure 3 shows the pressure distribution at the same cross-section, also showing Hexadap results on the unrefined coarse and fine meshes. The primary vortex is well-resolved by both methods, whereas the DG solver resolves a slightly stronger secondary vortex on the fine mesh due to the increased number of degrees of freedom.

Next the effectivity of the grid adaptation is demonstrated in Figure 4. At a cross-sectional plane parallel to the yz-plane at $x/c = 1.1$ (one tenth of the span behind the delta wing) the vortex system is compared for the simulation on the unrefined coarse mesh and the refined coarse mesh. The vortex system consists of vortices emanating from the leading edge of the delta wing and vortices shed from the thick trailing edge. In the figure the helicity $u \cdot \omega$ is plotted to distinguish counter-rotating vortices. The results on the unrefined mesh are shown on the left (mirrored in the symmetry plane), the results on the adapted mesh are shown on the right. Resolution of flow features is clearly increased, so it is concluded that the adaptive capability of the DG method is maintained for viscous flow simulation.

3.2 Laminar dynamic stall Dynamic stall may occur at high-speed conditions on the retreating blade since the local angle of attack is large at these positions. Dynamic stall is a complicated three-dimensional phenomenon and correct prediction of dynamic stall requires accurate prediction of turbulence, transition, and flow separation. Moreover, since massive flow separation may occur standard RANS turbulence models are probably not sufficiently accurate to capture the wake, and hybrid RANS-LES methods may be needed.

Here, the *laminar* two-dimensional flow around a NACA0012 airfoil in rapid pitch-up maneuver is considered. The flow conditions are identical to one of the conditions considered in Visbal et al. [16] and Osswald et al. [8], but the NACA0015 airfoil is replaced by the NACA0012 airfoil. The Reynolds number is 10,000 and the Mach number is 0.2. The evolution of the angle of attack α is described by $\alpha(t^+) = \omega^+ t^+ + \omega_0^+(1 - e^{-at^+}))$, where $t^+ = ta_\infty/c$ is the dimensionless time, $\omega^+ = \omega c/a_\infty$ is the reduced frequency. The second term in the definition of the angle of attack evolution is added to have zero initial velocity. After a short transition, the airfoil rotates at a constant angular velocity ω.

An initial mesh with 4256 cells has been generated. During the simulation the grid is refined at each time

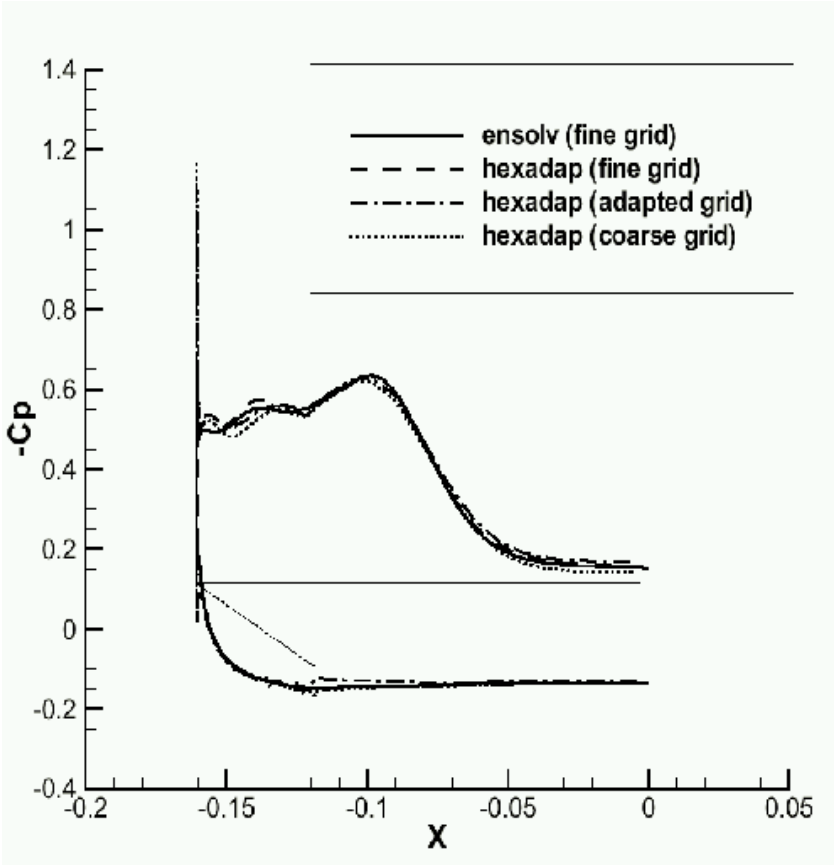

Figure 3: Vortex flow over a delta wing (Re=40,000, M=0.3, $\alpha = 12.5^o$). Comparison of pressure coefficient at a cross section of 60% chord between the DG solver Hexadap and the finite volume solver ENFLOW. For Hexadap results are also shown on the unadapted coarse and fine meshes.

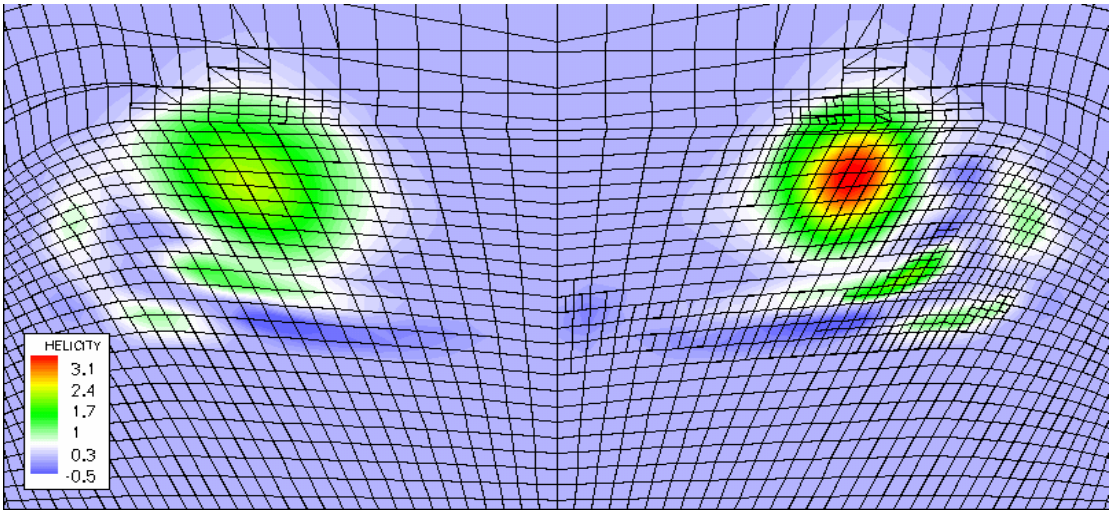

Figure 4: Vortex flow over a delta wing (Re=40,000, M=0.3, $\alpha = 12.5^o$). Comparison of vortex resolution at 10% span after trailing edge. Left unadapted results, right adapted results.

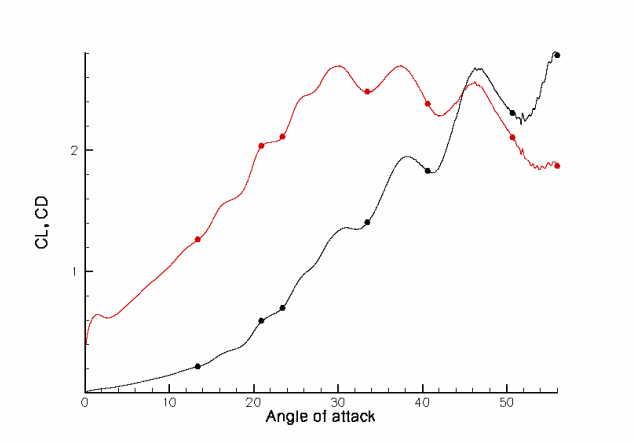

(a) CL, CD versus angle of attack

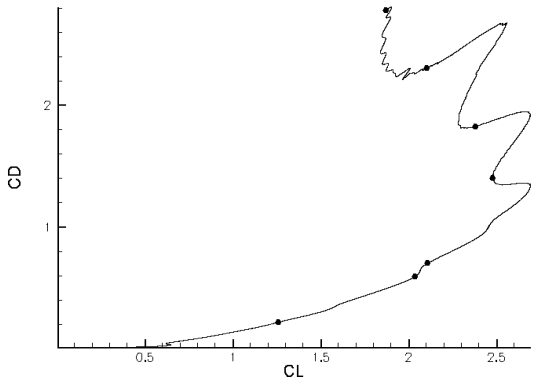

(b) CD versus CL

Figure 5: Evolution of lift and drag. The symbols are plotted at the angles of attack selected in Figures **??** and 6

step. A cell is refined whenever the vorticity magnitude is greater than a_∞/c and the mesh width is greater than $0.02c$. This refinement strategy aims at a uniform mesh of mesh width $0.01c$ in vorticity regions. The mesh evolution is shown in Figure **??**. Eventually the mesh contains 12,354 cells. The time step is equal to a change of 0.01 degrees in the angle of attack (after the transition period), a total number of 5000 time steps has been performed.

The evolution of the dynamic stall is shown in Figure 6. The separation of the boundary layer starts at the trailing edge and develops upstream ($\alpha = 13.4^o$). At an angle of attack $\alpha = 21.0^o$ separation near the leading edge occurs, and shortly afterwards ($\alpha = 23.5^o$) the complete boundary layer is separated into different vortices. The vortex system develops further ($\alpha = 33.5^o$) until the vortex near the leading edge separates from the airfoil ($\alpha = 40.7^o$) resulting in loss of lift (compare Figure 5). The stronger leading edge vortex flows downstream, causing some of the smaller vortices to rotate about it ($\alpha = 50.7^o$). The simulation is stopped at an angle of attack $\alpha = 56.0^o$, where the next trailing edge vortex has separated from the airfoil.

The evolution of lift and drag is shown in Figure 5, showing the loss of lift once the primary leading edge vortex has separated from the airfoil (at thirty degrees). Maximum lift is 2.7. The qualitative behaviour of the simulation is very similar to the behaviour described in Visbal et al. [16]. This simulation clearly demonstrates the capabilities of the viscous DG method for time-accurate simulations on deforming and adaptive meshes, which, as explained, is a necessary prerequisite for rotor simulations.

4 Conclusions and future work

The level of external vibratory loads is important for many operational aspects of helicopters. For the prediction of these loads a predictive tool based on first-principles physics has been studied. The aerodynamic module of the tool has been extended to model viscous effects. Viscous effects play a significant role in the aerodynamics of helicopter rotors in high-speed forward flight. The new model has been applied to three-dimensional vortex flow and laminar dynamic stall. The applications have clearly demonstrated the capability of the new model to perform on deforming and adaptive meshes.

The new aerodynamic module will be incorporated in NLR's framework for aero-elastic simulations of trimmed rotor systems in forward flight. The solution algorithm MTMG is independent of the type of equations being solved, hence its benefits will be unaffected by changing the aerodynamic model from inviscid to viscous

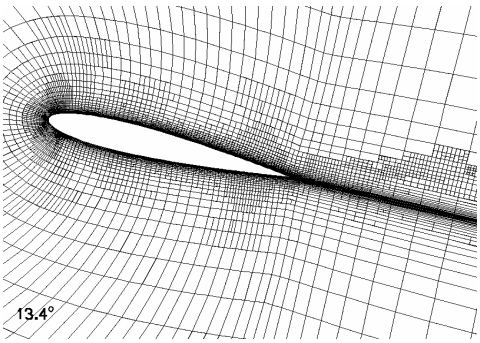

(a) $\alpha = 13.4^o$

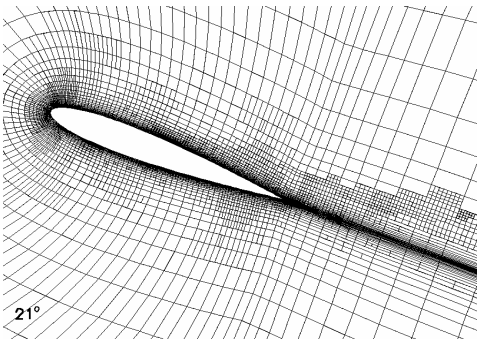

(b) $\alpha = 21.0^o$

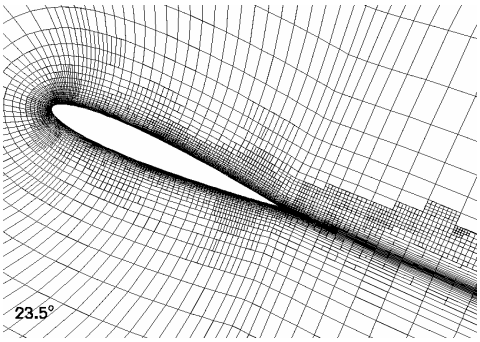

(c) $\alpha = 23.5^o$

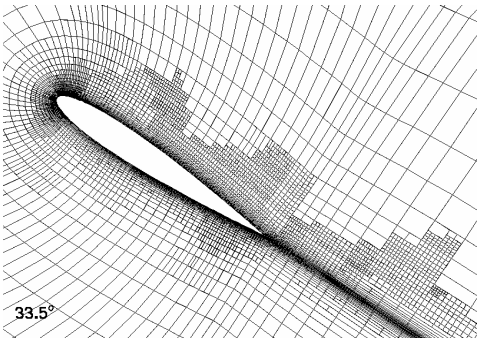

(d) $\alpha = 33.5^o$

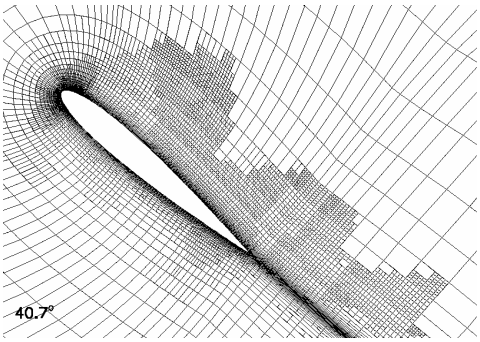

(e) $\alpha = 40.7^o$

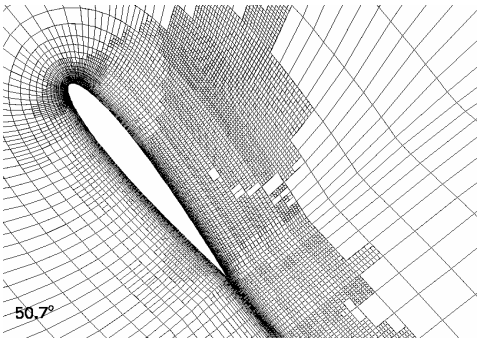

(f) $\alpha = 50.7^o$

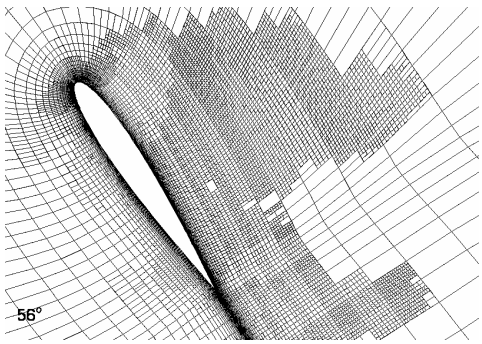

(g) $\alpha = 56.0^o$

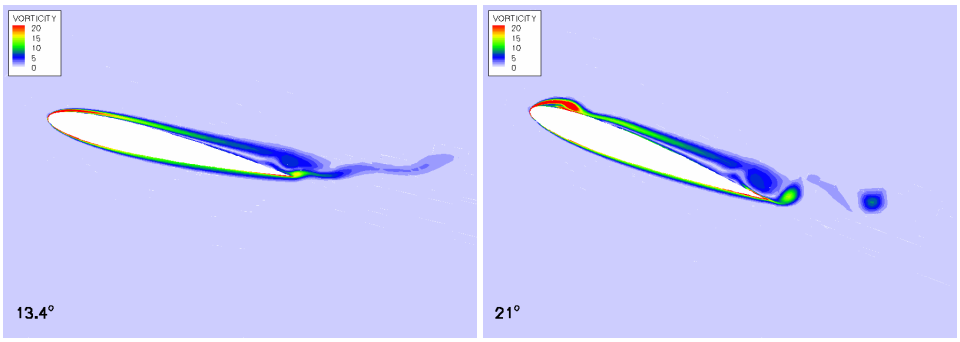

(h) separation starts at trailing edge

(i) leading edge separation

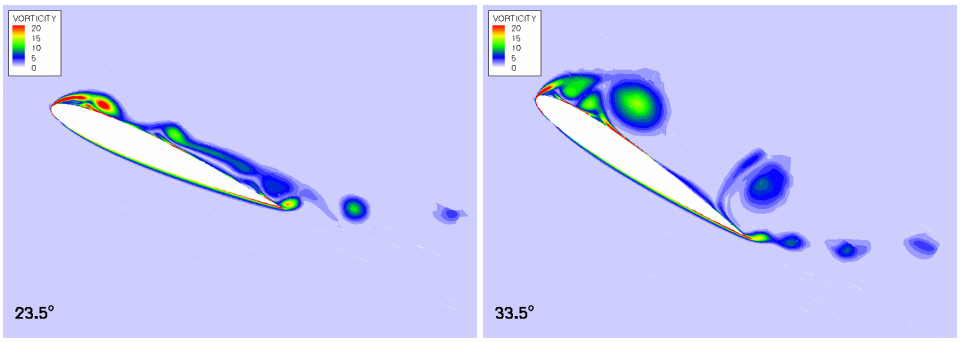

(j) boundary layer separates into several vortices

(k) vortices grow

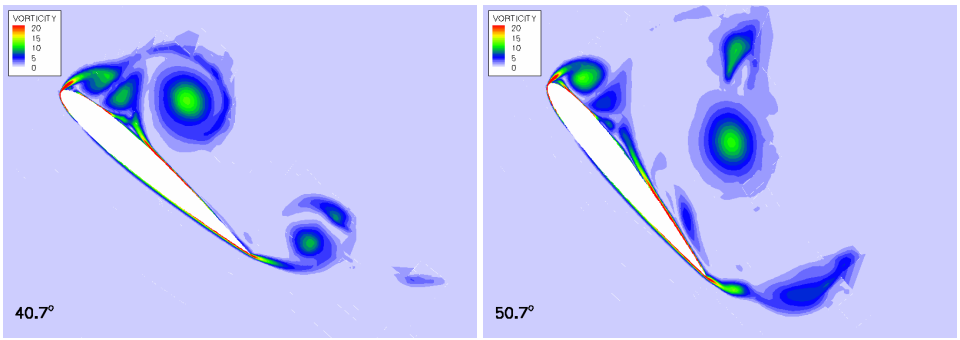

(l) leading edge vortex separates from airfoil

(m) rotating vortices

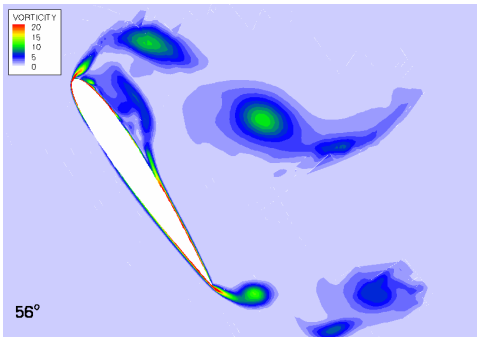

(n) end of simulation

Figure 6: Laminar dynamic stall for a NACA0012 airfoil (Re=10000, M=0.2). Vortex evolution

flows.

References

[1] T.J. Barth and H. Deconinck, editors. *High-order methods for computational physics*, volume 9 of *Lecture Notes in Computational Science and Engineering*. Springer Verlag, Berlin, 1999.

[2] O.J. Boelens, H. van der Ven, B. Oskam, and A.A. Hassan. Boundary conforming discontinuous Galerkin finite element approach for rotorcraft simulations. *J. of Aircraft*, 39 (5):776–785, sep-oct 2002.

[3] B. Cockburn. Discontinuous Galerkin methods for convection-dominated problems. In *[1]*, pages 69–224, 1999.

[4] O. Dieterich, H.-J. Langer, G. Imbert, M.H.L. Hounjet, V. Riziotis, O. Schneider, I. Cafarelli, R. Calvo Alonso, C. Clerc, and K. Pengel. HeliNOVI: Current Vibration Research Activities. In *Proceedings of the 31st European Rotorcraft Forum, September 13-15, 2005, Florence*, 2005.

[5] H. Hansen, P. Thiede, F. Moens, R. Rudnik, and J. Quest. Overview about the European high lift research programme EUROLIFT. In *42nd AIAA Aerospace Sciences Meeting and Exhibit*, number AIAA-2004-767, Reno, 5-8 January, 2004.

[6] C.M. Klaij, J.J.W. van der Vegt, and H. van der Ven. A space-time discontinuous Galerkin finite element discretization for the compressible Navier-Stokes equations. *submitted to J. Comp. Phys.*, 2005.

[7] J. C. Kok and S. P. Spekreijse. *Efficient and accurate implementation of the k-ω turbulence model in the NLR multi-block Navier-Stokes system*. NLR TP-2000-144 (presented at ECCOMAS 2000, Barcelona, Spain, 11-14 September, 2000), 2000.

[8] G.A. Osswald, K.N. Ghia, and U. Ghia. Simulation of dynamic stall phenomenom using unsteady Navier-Stokes equations. *Comp. Phys. Comm.*, 65:209–218, 1991.

[9] K. Pahlke and B. van der Wall. Calculation of multibladed rotors in high-speed forward flight with weak fluid-structure-coupling. In *Proceedings of the 27th European Rotorcraft Forum, September 11-14, 2001, Moscow*, 2001.

[10] K. Pahlke and B. van der Wall. Progress in weak fluid-structure-coupling for multibladed rotors in high speed forward flight. In *Proceedings of the 28th European Rotorcraft Forum, September 17-20, 2002, Bristol*, 2002.

[11] H. Pomin and S. Wagner. Aeroelastic analysis of helicopter rotor blades on deformable Chimera grids. *J. of Aircraft*, 41(3):577–584, 2004.

[12] A.J. Riley and M.V. Lowson. Development of a three dimensional free shear layer. *J. Fluid Mech.*, 369:49–89, 1008.

[13] G. Servera, P. Beaumier, and M. Costes. A weak coupling method between the dynamics code HOST and the 3D unsteady Euler code WAVES. In *Proceedings of the 26th European Rotorcraft Forum, September 26-29, 2000, The Hague*, 2000.

[14] J.J.W. van der Vegt and H. van der Ven. Space-time discontinuous Galerkin finite element method with dynamic grid motion for inviscid compressible flows. Part I. General formulation. *J. Comput. Phys.*, 182:546–585, 2002.

[15] H. van der Ven and O.J. Boelens. A framework for aeroelastic simulations of trimmed rotor systems in forward flight. In *proceedings of the 30th European Rotorcraft Forum, Marseille, September 14-16, 2004*, 2004.

[16] M.R. Visbal and J.S. Shang. Investigation of the flow structure around a rapidly pitching airfoil. *AIAA Journal*, 27(8):1044–1051, 1998.